Photocatalytic degradations of malachite green on magnetically separable $Ni_{1-x}Co_xFe_2O_4$ nanoparticles synthesized by using a hydrothermal process

H- Y. He

College of Material Science and Engineering, Shaanxi University of Science and Technology, Xi'an, Shaanxi, China(710021)

**Corresponding Author: E-mail: hehy@sust.edu.cn, Fax:0086-29-86168803; Tel: 0086-15319453608*

Abstract: $Ni_{1-x}Co_xFe_2O_4$ (x=0–1.0) ferrite nanoparticles were synthesized by using a hydrothermal process. The nanoparticles had average particle sizes of 14.8−29.4 nm and a narrow band gap of 1.75−1.91 eV, decreasing with increasing Co content. The nanoparticles showed an excellent sunlight-excited photocatalytic activity to malachite green in water. Moreover, the addition of a small amount of H_2O_2 resulted in an obviously enhanced photodegradation, indicating a Fenton-like reaction. The photodegradation and Fenton-like photodegradation rates increased with increasing Co content. Complete Co substitution for Ni resulted in an optimal effect. Quasi-kinetic rate constant *k* values were in the range of $2.23–7.2\times10^{-2}$ min^{-1} and increased to $1.3–6.0\times10^{-1}$ min^{-1} upon the addition of H_2O_2. The measurement of oxidation-reduction potential of the nanoaprticles in the photodegradation condition indicated a reductive characteristic enhanced with increasing Co content. Furthermore, the nanoparticles possessed high saturation magnetizations of 50.7−64.2 $emu\cdot g^{-1}$ and low coercivity of 0.4−1.7 kOe, which ensure that they gave magnetic separable in finally degraded dye aqueous solution.

Keywords: Nanostructure; semiconductors; dye photodegradation; Fenton-like reaction; magnetic separation

1. Introduction

Photocatalysis plays an important role in dealing with today's challenging demand for decontamination of environment. For this purpose, nano-TiO_2 as a photocatalyst has been widely studied because of its excellent chemical stability and photocatalytic activity. To fully utilize sunlight and enhance the photocatalytic activity of nano-photocatalyst, developing photocatalyst with narrower band gap semiconductor than pure TiO_2 should be of interest In some cases, such as waste water treatment, photocatalyst nanoparticles are also required to be separated from the photodegraded aqueous solution after the photodegradation process is completed. Magnetic separation is generally believed to be an effective technique.

Spinel ferrites have narrow band gap (~2.0 eV), so their nanoparticles could be potential photocatalyts for decontamination of environment because of their superiority in full utilization of natural sunlight. Moreover, this type of ferrites are ferrimagnetic and thus magnetic separable from aqueous solution. Previous studies have shown the excellent photocatalytic activity of some ferrite nanoparticles [1, 2]. Recent studies further indicated that the composites of different ferrites [2] and ferrite with other photocatalysts [3, 4] have higher efficiency than single ones. Different metal cations have different physical chemical behavior. Thus, it is necessary to investigate the effect of Co substitution for Ni on photocataytic activity of nickel

ferrite nanoparticles.

In recent years, advanced oxidation processes (AOPs) by using UV/H_2O_2 have become a way to degrade organic compounds in dilute solutions. In general, it is believed that the UV/H_2O_2 processes result in the formation of OH radicals in solution, which accelerate the oxidation degradation of the organic compounds in water. The use of H_2O_2 has a main disadvantage of high cost, whereas the low oxidation rate is the major draw back of semiconductors, such as TiO_2. The combined use of H_2O_2 and semiconductors is a way of solving this problem. Many studies have been devoted to the examination of organic compound photodegradation in the presence of H_2O_2 and TiO_2 [5,6]. This process is usually called Fenton-like process because it is similar to the advanced oxidation process based on the homogeneous Fenton reagent (Fe^{2+}/H_2O_2) or Fenton-like (Fe^{3+}/H_2O_2) [7,8]. Up to now, various Fenton and Fenton-like processes have been used for the degradation of organic pollution. For example, activated carbon fibers [9], impure bismuth ferrite [10], copper slag (90% Fe_2SiO_4) [11], ferrioxalate complexes [12], iron/ordered mesoporous carbon catalyst [13], iron oxide nanotube layer [14], Cu^{2+} [15], et al. Have be used as a Fenton-type photocatalyst or assisted Fenton-type photocatalysts. However, the photocatalytic and Fenton-like photocatalytic activities of $Ni_{1-x}Co_xFe_2O_4$ ferrite nanoparticles have not been reported as dye removal from waste water..

To date, many methods have been developed to synthesize spinel ferrite nanoparticles, such as aerosol route [16], co-precipitation method [17, 18], ceramic technique [19], hydrolysis method [20], microwave-hydrothermal method [21], and

hydrothermal method [22]. The hydrothermal process has be widely used to synthesize the spinel ferrites because of its simple process, low cost, low synthesis temperature and small particle size [22].

In this study, we focus on hydrothermal synthesis of $Ni_{1-x}Co_xFe_2O_4$ nanoparticles, examining the effect of Co content on microstructure, photocatalytic activity for malachite green removal from aqueous solution, and magnetic property of the nanoparticles.

2. Experimental

Nickel chloride ($NiCl_2 \cdot 6H_2O$, Shenyang Hua Bai Tai Chemical Co. Ltd., China), cobalt chloride ($CoCl_2 \cdot 6H_2O$, Hebei Kingway Chemical Co. Ltd., China), and iron nitrate ($Fe(NO_3)_3 \cdot 9H_2O$, Beijing Baishunchem. Co. Ltd., China) were used as starting materials. The starting materials were all analytical agent without further processing. The starting materials were first weighed according to the compositions of $Ni_{1-x}Co_xFe_2O_4$ (x=0, 0.2, 0.4, 0.6, 0.8, and 1.0) and dissolved in 15 mL deionic water. The solutions have Fe^{3+} concentration of 0.02 mol L^{-1}. The solutions were then transferred into autoclaves (volume: 25 mL). Subsequently, NaOH with fourfold gram equivalent of all metal cations was dissolved in deionic water (5 mL) and added dropwise into the metal cation aqueous solutions with constant magnetic stirring. The use of excess NaOH can assure full precipitation of all cations. After sealing, hydrothermal reaction was carried out in a hydrothermal oven at 180 ℃ for 24 h. Heating rate was about 30 ℃·min^{-1}. After naturally cooling in the oven, the products were finally washed repeatedly with distilled water, and then dried at 100 ℃ for 24

h.

Phase composition of the $Ni_{1-x}Co_xFe_2O_4$ nanoparticles was identified by using X-Ray diffractometer (XRD, $CuK_{\alpha1}$, λ=0.15406nm, Model No: D/Max--2200PC, Rigaku, Japan). Morphology of the nanoparticles was analyzed by using scanning electron microscope (SEM, Model No: JXM-6700F, Japan). Fourier transform infrared spectra of the nanoparticles were measured with Fourier transform infrared spectrometer (FTIR, Model no: VERTEX 70, Bruke, German). KBr was used as matrix to disperse the ferrite nanoparticles for compressing disk sample. Absorbance spectra of the nanoparticles were determined with an ultraviolet-visible spectrophotometer (Model No: 722, Hengping, China). Magnetic property was measured with a vibrating sample magnetometer (VSM, Model No: Versa Lab, Quantun Design, USA)

To study the photocatalytic and photo-Fenton like degradation of malachite green in a water on the nanoparticles, malachite green aqueous solution with a concentration of 1×10^{-6} M was first prepared. In each experiment, 50 mL malachite green aqueous solution and 25 mg the ferrite nanoparticles were added into a glass beaker with constant stirring for 1-2 min. The photocatalysis experiment was carried out under the irradiation of sunlight. The intensity of sunlight reaching the surface of the solutions measured with a solar power meter (Model no: SM206, China) was ~250 $W\cdot m^{-2}$. After leaving to steady state in dark for 10 min and at each irradiation interval, ~3 mL solutions were took out and filtrated out the suspended tiny particles and subsequently measured to check their absorbance on a spectrophotometer (Model No: 722N,

112 Hengping, China). The solutions after the test were returned to the beakers to
113 maintain the normal volume of the solutions under test. Similar experiment was
114 carried out by adding 0.5 mL H_2O_2 into each of the 50 mL dye aqueous solution.

115 In first hour of the above processes, the oxidation-reduction potential (ORP) of the
116 malachite green aqueous solutions with and without the photocatalyts was determined
117 by using an oxidation-reduction potential tester (ORP-286, China). The ORPs of the
118 nanoparticle surfaces in the condition of dye photodegradation were estimated by
119 calculating the differences between the measured ORP of the dye aqueous solutions
120 with and without the nanoparticles. The absorbance and ORP of the dye aqueous
121 solutions were all the average value of two repeated measurement values

122

123 **3. Results and discussion**

124 **3.1. XRD analysis**

125 Figure 1a shows XRD patterns of the synthesized nanoparticles. All diffraction
126 peaks match with the diffraction data of spinel ferrites. This indicates that the
127 nanoparticles are single phase. The intensity of the XRD peaks first slightly decreases
128 when the Co content (x) is increased from 0 to 0.8 and then increases with further
129 cobalt substitution, drawing out variation tend in crystallinity of the nanoparticles.
130 This decrease trend of the crystallinity with cobalt substitution was also reported for
131 the $Ni_{1-x}Co_xFe_2O_4$ nanoparticles synthesized by using solvothermal route [23]. This
132 could be mainly due to smaller radium difference (0.72–0.64 Å) between Ni^{2+} and
133 Fe^{3+} ions than that (0.74–0.64Å) between Co^{2+} and Fe^{3+} ions. The smaller radium

difference leads to smaller inhibition of Ni^{2+} substitution for Fe^{3+} to the spinel crystal growth than Co^{2+} substitution. Moreover, the position of strongest peak (311) shifts to lower 2θ with Co substitution (Fig. 1b). This can be ascribed to the increase in the interplanar crystal spacing (*d*) based on Bragg's equation. The lattice parameter of the nanoparticles with cubic crystal structure can be calculated by following equation with the XRD analysis data:

$$\frac{a^2}{d^2} = h^2 + k^2 + l^2 \quad (1)$$

Calculated *a* values are 0.8236 nm, 0.8263 nm, 0.8298 nm, 0.8321 nm, 0.8339 nm and 0.8377 nm for the Co content x=0, 0.2, 0.4, 0.6, 0.8, and 1.0, respectively (Fig. 1c). This indicates the expansion of the lattice with the cobalt substitution, agreeing with the shift of (311)-peak. Similar lattice parameter variation was also reported in previous literature [16, 24]. Moreover, the lattice parameter *a* of $CoFe_2O_4$ equals to 0.8391 nm (JCPDS: 22-1086) that is larger than 0.83379 nm (JCPDS: 74-2081) and 0.83390 nm (JCPDS: 10-0325) of the $NiFe_2O_4$. Furthermore, the lattice parameter of the all ferrites is smaller than the value given in the JCPDS card, especially as the Co content approaches zero. This could be ascribed to the high-pressure effect in the condition of hydrothermal synthesis. Similarly, the lattice parameter of the $NiFe_2O_4$ nanoparticle is smaller when they were synthesized by using hydrothermal process than sol-gel method [25]. The average crystal sizes of the nanoparticles are determined from XRD data with Debye–Scherrer's formula [26]:

$$D = \frac{0.9\lambda}{\beta \cos\theta}$$

where λ is the X-ray wavelength, β the full width at half maximum (FWHM) of the

156 considered peak and θ is the Bragg angle. The results are 23.4, 29.4, 23.6, 19.4, 16.5,
157 and 14.8 nm for the x=0, 0.2, 0.4, 0.6, 0.8 1.0, respectively.

158 **3.2. SEM**

159 Figure 2 shows SEM micrographs of the nanoparticles. Most of the nanoparticles
160 show spherical morphology with some agglomeration (Fig. 2c–2f), while the
161 $Ni_{1-x}Co_xFe_2O_4$ (x=0.8 and 1.0) nanoparticles have approximately cubical morphology
162 (Fig. 2a and 2b). This could be mainly due to same reason of the difference in
163 crystallinities of the nanoparticles. From the SEM micrographs, the average particle
164 sizes are also increased as increasing x from 0 to 0.8 and then decreased with further
165 cobalt substitution. The sizes of the nanoparticles with x=0.8 and 1.0 are obviously
166 larger than the results of XRD analysis, which means that these nanoparticles are
167 polycrystalline.

168 **3.3. FTIR analysis**

169 Figure 3 shows FTIR spectra of the nanoparticles. The peak centered at ~3416 cm^{-1}
170 is attributed to the stretching vibration of surface hydroxyls absorbed on surface and
171 O–H groups in absorbed water [27]. The peak centered at 1620 cm^{-1} is assigned to the
172 H–O–H bending vibration in water molecular [28] or the OH deformation vibration
173 due to surface hydroxyls [29, 30]. These imply good nanoparticle surface
174 hydrophilicity that may be favorable for the photocatalytic activity. The weak peak at
175 1124 cm^{-1} could be assigned to the C–O stretching [31] due to the adsorbed CO_2. The
176 two peaks at ~483 cm^{-1} and ~616 cm^{-1} are assigned to the vibrations of ferrite groups
177 [32], corresponding to the octahedral and tetrahedral sites of positive ions in the

178 ferrite, respectively [28, 33]. The difference in absorption positions between the
179 octahedral and tetrahedral complexes of the $Ni_{1-x}Co_xFe_2O_4$ crystals is due to the
180 different distances between Fe^{3+}–O^{2-} in the octahedral and tetrahedral sites. This
181 confirms the formation of single phase $Ni_{1-x}Co_xFe_2O_4$ structure.

182 **3.4. Optical absorption**

183 Figure 4 shows absorbance spectra of the ferrite nanoparticles. The absorbances in
184 UV-visible region are large and increase with increasing Co content. The estimated
185 absorption edge increases from ~648 nm to ~710 nm. Accordingly, the band gap
186 energies of the nanoparticles decrease from ~1.91 eV to ~1.75 eV (Inserted figure in
187 Fig. 4).

188 **3.5. Photocatalytic degradation of the dye in a water**

189 Figure 5 shows concentration variations of the malachite green aqueous solutions on
190 the nanoparticles with the irradiation time of sunlight. The degradation rate increases
191 with increasing Co content. This increase of degradation rate could be ascribed to the
192 decrease of band gap and average particle size and the increase of light absorbance of
193 nanoparticles as the increase of Co content. In addition, the ORP values are negative
194 and decrease (Fig. 6). This indicates that the nanoparticles surface are dominantly
195 reductive in the photocatalysis condition, This characteristics is enhances with
196 increasing Co content.

197 **3.6. Fenton-like photodegradation of the dye in a water on the nanoparticles**

198 Figure 7 shows concentration variations of the malachite green aqueous solution
199 with H_2O_2 on the nanoparticles with the irradiation time of sunlight. The degradation

is obviously faster than that without H_2O_2, which indicates a significant photo-Fenton-like reaction. Similarly, the degradation rate increases as the Co content is increased. This increase could also be ascribed to the decrease of band gap and average particle size and the increase of light absorbance. The photo-generated electron-hole pairs in the nanoparticles could play similar role of Fe^{2+} and Fe^{3+} in Fenton reaction. The concentration increase in photo-generated electrons and holes leads to the enhanced photo-Fenton-like reaction. The ORP values in this process are larger than those in the cases without H_2O_2. The ORP also shows a nonlinear variation with Co contents, (Fig. 6). The difference and variation of ORP could be related to the surface characteristics of the nanoparticles, the acidic-alkaline behavior of the dye, oxidation of H_2O_2 and Fenton-like reaction.

Kinetic relation between concentration (C) of the malachite green aqueous solution and photocatalytic reaction time (t) can be given by:

$$\frac{C_0}{C} = \mathrm{A}\exp\left(\frac{kt}{T}\right)$$

where C_0 is initial concentration, k is quasi-kinetic rate constant, T is reaction temperature and A is a constant. Fig. 8 shows the plots of $\ln(C/C_0)$ versus t. The plots are approximately linear. The k values can be estimated directly from the plots. The estimated k values are in the range of $2.23–7.2\times10^{-2}$ min^{-1}, which is increased nearly one order of magnitude to $1.3–6.0\times10^{-1}$ min^{-1} as H_2O_2 is used. The k values increase with increasing Co content in both cases with and without H_2O_2.

3.7. Magnetic property of the nanoparticles

Figure 9a show room temperature hysteresis loops of the $Ni_{1-x}Co_xFe_2O_4$ nanoparticles. The nanoparticles are all ferrimagnetic. With increasing applied field, the magnetization of the $Ni_{1-x}Co_xFe_2O_4$ nanoparticles increases, and reaches saturation state under highest applied magnetic fields of 30 kOe. Maximum value of magnetization at applied field of 30 KOe (saturation magnetization *M*s) is in the ranges of 50.7−64.2 emu·g^{-1} (Fig. 9b). The coercivity (H_c) is in the range of 0.4−1.7 kOe (Fig. 9b). The ferrite nanoparticles with Co content x=0.8 show maximal Ms and Mr. This can be mainly ascribed to the maximal cation distribution of Fe^{3+} and Co^{2+} at the octahedral site (B-site) since the magnetic moments of Zn^{2+}, Co^{2+} and Fe^{3+} are 0 μB, 3 μB and 5 μB, respectively. Other reasons include the difference in particle size, easy magnetization axis and shape anisotropy. The large *M*s and low *H*c can provide excellent magnetic separation performance for the ferrite nanoparticles in the final degraded dye aqueous solution.

4. Conclusions

Single phase $Ni_{1-x}Co_xFe_2O_4$ (x=0.1−1.0) ferrite nanoparticles showed high photocatalytic activity in the sunlight-excited photodegradation of malachite green in a water. The addition of small amount of H_2O_2 resulted in remarkably enhanced photodegradation, indicating the present of Fenton-like reaction. Due to the increases in light absorbance and the decrease in band gap and average particle size, the photodegradation and Fenton-like photodegradation rates increased wiht increasing Co content. The ferrite nanoparticles also showed high satuation magnetizations and

low coercivities, which can provided excellence magnetic separation performance for the nanoparticles.

Acknowledgements: The authors thank the Mr. H. Tian of the Northwest Institute for Non-Ferrous Metal Research for his kind assistance in SEM measurement

References

[1] P.-G Guo, G.-L. Zhang, J.-Q. Yu, H.-L. Li, X.-S. Zhao, Controlled synthesis, magnetic and photocatalytic properties of hollow spheres and colloidal nanocrystal clusters of manganese ferrite, Colloids and Surf., A 395 (2012) 168-174

[2] E. Casbeer, V.K. Sharma, X.-Z. Li, Synthesis and photocatalytic activity of ferrites under visible light: A review, Sep. Purif. Technol. 87 (5) (2012) 1-14

[3] A.A. Aziz, K.S. Yong, S. Ibrahim, S. Pichiah, Enhanced magnetic separation and photocatalytic activity of nitrogen doped titania photocatalyst supported on strontium ferrite, J. Hazard. Mater. 199–200 (15) (2012) 143–150

[4] Y.-S. Fu, H.-Q. Chen, X.-Q. Sun, X. Wang. Combination of cobalt ferrite and graphene: High-performance and recyclable visible-light photocatalysis, Appl. Catal. B: Environ. 111–112 (12) (2012) 280-287

[5] Adrián M.T. Silva, Ekaterini Nouli, Nikolaos P. Xekoukoulotakis and Dionissios Mantzavinos, Effect of key operating parameters on phenols degradation during H_2O_2-assisted TiO_2 photocatalytic treatment of simulated and actual olive mill wastewaters, Appl. Catal. B: Environ. 73(1–2)(2007) 11–22

[6] Emad S. Elmolla, and Malay Chaudhuri, Photocatalytic degradation of amoxicillin, ampicillin and cloxacillin antibiotics in aqueous solution using UV/TiO_2 and UV/H_2O_2/TiO_2 photocatalysis, Desalination 252(1–3) (2010) 46–52

[7] Neamtu M, Zaharia C, Catrinescu C, Yediler A, Macoveanu M, Kettrup 1 A, Fe-exchanged Y zeolite as catalyst for wet peroxide oxidation of reactive azo dye Procion Marine H-EXL, Appl Catal B: Environ. 48 (2004) 287–294.

[8] Guelou E, Barrault J, Fournier J, Tatibouet JM, Active iron species in the catalytic wet peroxide oxidation of phenol over pillared clays containing iron, Appl Catal B: Environ. 44 (2003) 1–8.

[9] Lie Wang, Yuyuan Yao, Zhanhao Zhang, Lijie Sun, Wangyang Lu, Wenxing Chen, Haixiang Chen, Activated carbon fibers as an excellent partner of Fenton catalyst for dyes decolorization by combination of adsorption and oxidation, Chem. Eng. J. 251 (2014) 348–354

[10] Tayyebe Soltani, Mohammad H. Entezari, Solar-Fenton catalytic degradation of phenolic compounds by impure bismuth ferrite nanoparticles synthesized via ultrasound, Chem. Eng. J. 251 (2014) 207–216

[11] M. Solís-López, A. Durán-Moreno, F. Rigas, A.A. Morales, M. Navarrete, R.M. Ramírez-Zamora, Assessment of copper slag as a sustainable Fenton-type photo-catalyst for water disinfection, Water Reclamation and Sustainability June (2014) 199–227

[12] Isabelli N. Dias, Bruno S. Souza, João H.O.S. Pereira, Francisca C. Moreira, Márcia Dezotti, Rui A.R. Boaventura, Vítor J.P. Vilar, Enhancement of the

288 photo-Fenton reaction at near neutral pH through the use of ferrioxalate
289 complexes: A case study on trimethoprim and sulfamethoxazole antibiotics
290 removal from aqueous solutions, Chem. Eng. J. 247 (2014) 302–313
291 [13] Feng Duan, Yuezhu Yang, Yuping Li, Hongbin Cao, Yi Wang, Yi Zhang,
292 Heterogeneous Fenton-like degradation of 4-chlorophenol using iron/ordered
293 mesoporous carbon catalyst, J. Environ. Sci. 26 (5) (2014) 1171–1179
294 [14] Jun-Won Jang, Jae-Woo Park, Iron oxide nanotube layer fabricated with
295 electrostatic anodization for heterogeneous Fenton like reaction, J. Hazard. Mater.
296 273 (30) (2014) 1–6
297 [15] Hye-Jin Lee, Hongshin Lee, Changha Lee, Degradation of diclofenac and
298 carbamazepine by the copper(II)-catalyzed dark and photo-assisted Fenton-like
299 systems, Chem. Eng. J. 245 (2014) 258–264
300 [16] T.E. Agustina, H.M. Ang, V.K. Vareek. A review of synergistic effect of photo-
301 catalysis and ozonation on wastewater treatment, J. Photochem. Photobiol. C:
302 Photochem. Rev. 6 (2005) 264–273
303 [17] V.L. Mathe, A.D.Sheikh. Magnetostrictive properties of nanocrystalline Co–Ni
304 ferrites, Physica B 405 (2010) 3594–3598
305 [18] R. Arulmurugan, G. Vaidyanathan, S. Sendhilnathan, B. Jeyadevan, Thermo-
306 magnetic properties of $Co_{1-x}Zn_xFe_2O_4$ (x=0.1–0.5) nanoparticles, J. Magn. Magn.
307 Mater. 303 (2006) 131−137.
308 [19] A. Tawfik, I.M. Hamada, O.M. Hemeda, Effect of laser irradiation on the
309 structure and electromechanical properties of Co–Zn ferrite, J. Magn. Magn.

Mater. 250 (2002) 77−82.

[20] G.V. Duong, N. Hanh, D.V. Linh, R. Groessinger, P. Weinberger, E. Schafler, M. Zehetbauer, Monodispersed nanocrystalline $Co_{1-x}Zn_xFe_2O_4$ particles by forced hydrolysis: Synthesis and characterization, J. Magn. Magn. Mater. 311 (2007) 46−50.

[21] C.-K. Kim, J.-H. Lee, S. Katoh, R. Murakami, M. Yoshimura, Synthesis of Co-, Co-Zn and Ni-Zn ferrite powders by the microwave-hydrothermal method, Mater. Res. Bull. 36 (2001) 2241−2250.

[22] F. Gözüak, Y. Köseoğlu, A. Baykal, H. Kavas, Synthesis and characterization of $Co_xZn_{1-x}Fe_2O_4$ magnetic nanoparticles via a PEG-assisted route, J. Magn. Magn. Mater. 321 (2009) 2170−2177.

[23] Y. Tang, X.-W. Wang, Q.-H. Zhang, Y.-Q. Li, H.-Z. Wang, Solvothermal synthesis of Co_{1-}xNixFe$_2O_4$ nanoparticles and its application in ammonia vapors detection, Progress in Natural Science: Materials International 22 (2012) 53–58

[24] R. Mukherjee, T. Sahu, S. Sen, P. Sahu, Structural and microstructural evolution due to increasing Co substitution in Ni_{1-}xCoxFe$_2O_4$: An X-ray diffraction study using the Rietveld method, Mater. Chem. Phys. 128 (2011) 365–370

[25] M. Srivastava, S. Chaubey, A.K. Ojha, Investigation on size dependent structural and magnetic behavior of nickel ferrite nanoparticles prepared by sol–gel and hydrothermal methods, Mater. Chem. Phys. 118 (2009)174–180

[26] H.P. Klug, L.E. Alexander, X-ray Diffraction Procedures for Polycrystalline and Amorphous Materials, 2nd ed., John Wiley & Sons, New York, 1974.

[27] S. Yáñez-Vilar, M. Sánchez-Andújar, C. Gómez-Aguirre, J. Mira, M.A. Señarís-Rodríguez, S. Castro-García, A simple solvothermal synthesis of MFe_2O_4 (M¼Mn, Coand Ni) nanoparticles, J. Solid State Chem. 182 (2009) 2685–2690.

[28] C.-H. Lu, S.-J. Liou, Hydrothermal preparation of nanometer lithium nickel vanadium oxide powder at low temperature, Mater. Sci. Eng., B 75 (2000) 38–42.

[29] P. Priyadharsini, A. Pradeep, P. Sambasiva Rao, G. Chandrasekaran, Structural, spectroscopic and magnetic study of nanocrystalline Ni–Zn ferrites, Mater. Chem. Phys. 116 (2009) 207–213

[30] X.-C. Shen, X.-Z. Fang, Y.-H. Zhou, H. Liang, Synthesis and characterization of 3-aminopropyltriethoxysilane-modified superparamagnetic magnetite nano-particles, Chem. Lett. 33 (2004) 1468–1469.

[31] M. Ma, Y. Zhang, W. Yu, H.-Y. Shen, H.-Q. Zhang, N. Gu, Preparation and characterization of magnetite nanoparticles coated by amino silane**,** Colloids Surf. A 212 (2003) 219–226.

[32] H. Sozeri, Z. Durmus, A. Baykal, Structural and magnetic properties of triethylene glycol stabilized $Zn_xCo_{1-x}Fe_2O_4$ nanoparticles. Mater. Res. Bull. 47 (2012) 2442–2448

[33] S.-H. Xiao, W.-F. Jiang, L.-Y. Li, X.-J. Li, Low-temperature auto-combustion

synthesis and magnetic properties of cobalt ferrite nanopowder, Mater. Chem. Phys. 106 (2007) 82–87.

Figures:

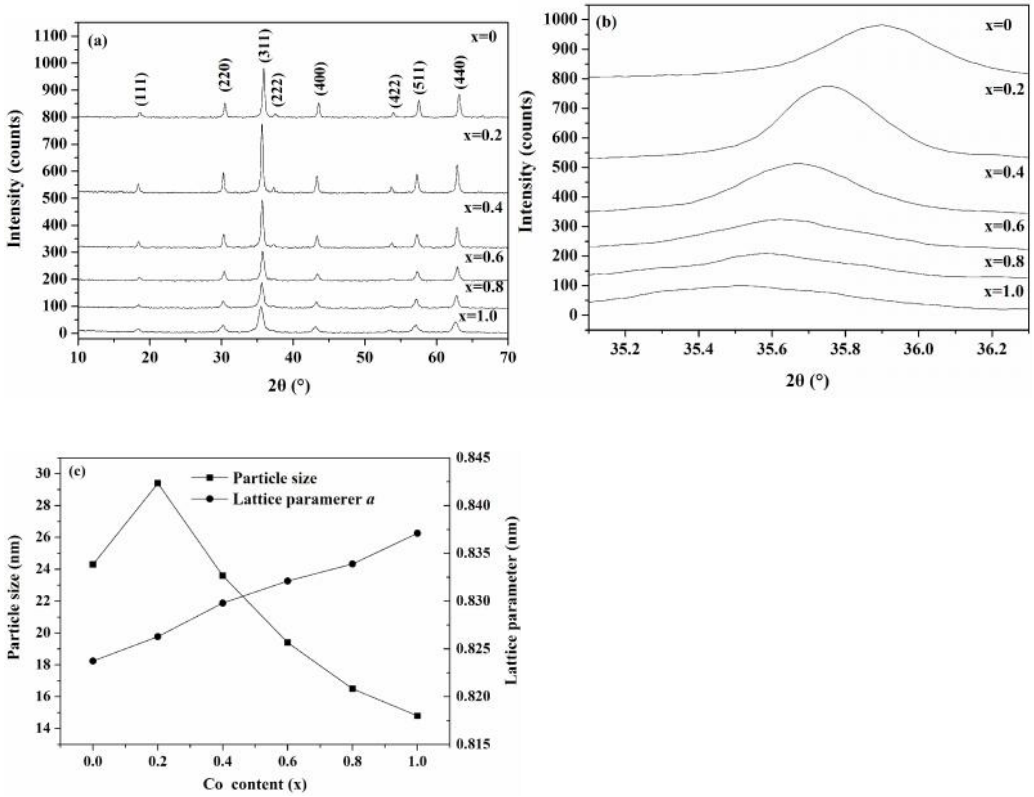

Figure 1. (a) XRD patterns and (b) Enlarged (311) peak in the XRD patterns (c) Average particle size and lattice parameter of the $Ni_{1-x}Co_xFe_2O_4$ nanoparticles.

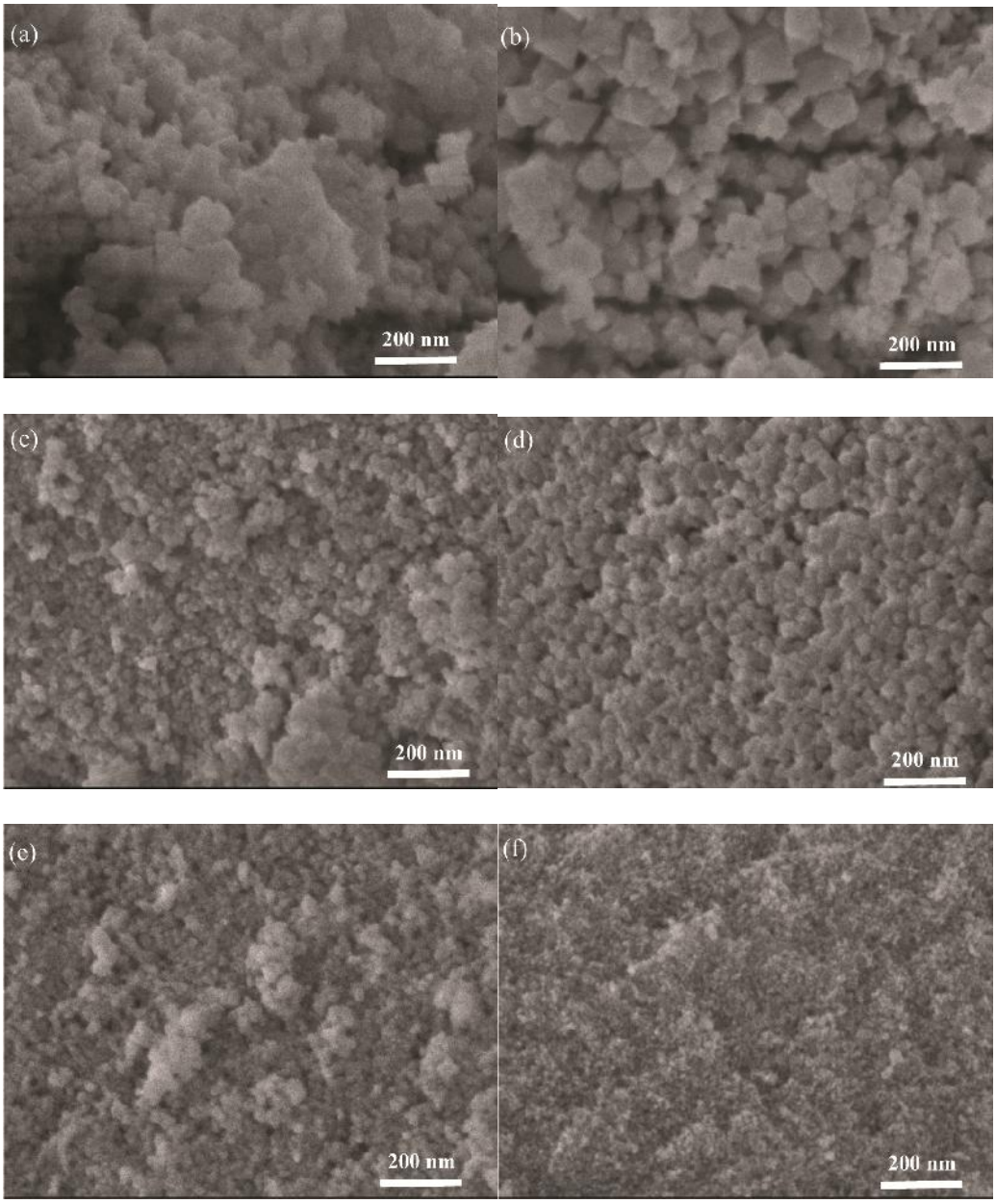

Figure 2. SEM micrographs of the $Ni_{1-x}Co_xFe_2O_4$ nanoparticles with various Co content (a) x=0, (b) x=0.2, (c) x=0.4, (d) x=0.6, (e) x=0.8, and (f) x=1.0.

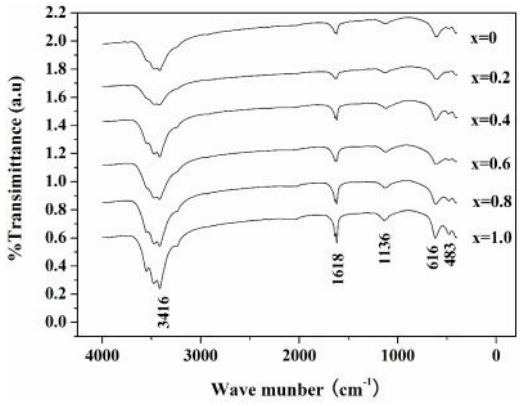

Figure 3. FTIR spectra of the $Ni_{1-x}Co_xFe_2O_4$ nanoparticles.

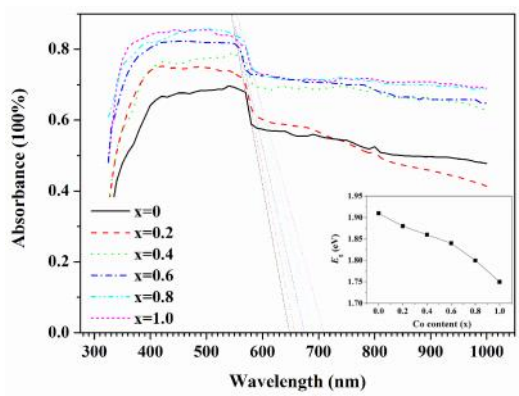

Figure 4. Absorbance spectra of the $Ni_{1-x}Co_xFe_2O_4$ nanoparticles. Inserted figure is the plots of band gap (E_g) *vs.* Co content (x).

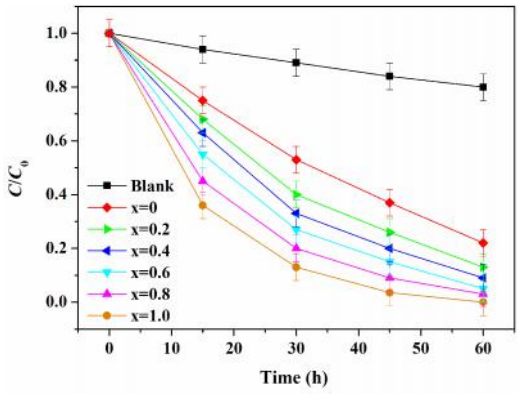

Figure 5. Concentration variations of malachite green aqueous solutions on the $Ni_{1-x}Co_xFe_2O_4$ nanoparticles with the irradiation time of sunlight.

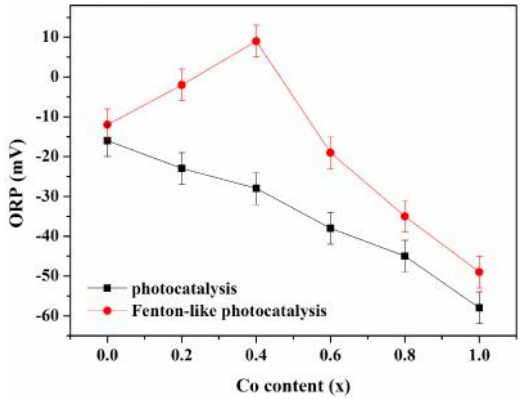

Figure 6. ORP variations of $Ni_{1-x}Co_xFe_2O_4$ nanoparticles with Co content (x) in the photocatalytic and photo-Fenton-like degradation systems.

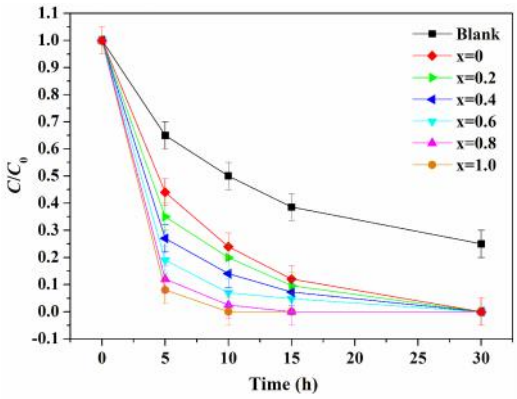

Figure 7. Concentration variations of malachite green aqueous solutions containing H_2O_2 (concentration equal 10 ml/l) on the $Ni_{1-x}Co_xFe_2O_4$ nanoparticles with the irradiation time of sunlight.

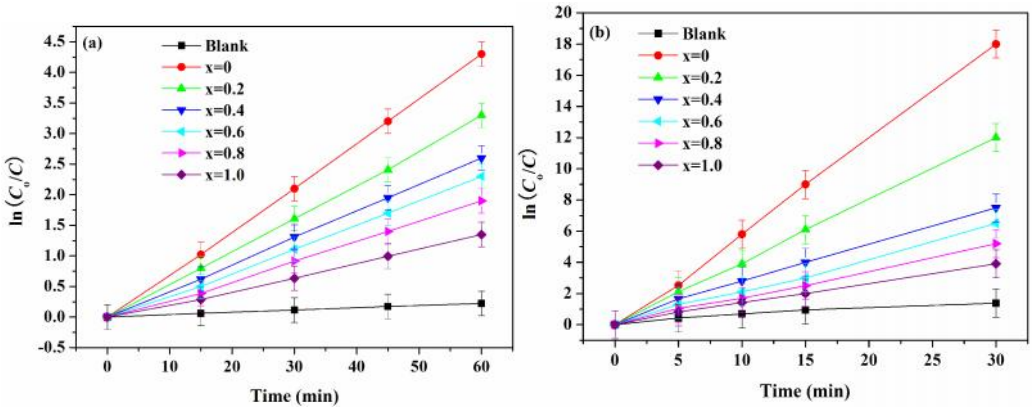

Figure 8. The plots of $\ln(C/C_0)$ vs. the irradiation time of sunlight in case of (a) H_2O_2-free and (b) using H_2O_2.

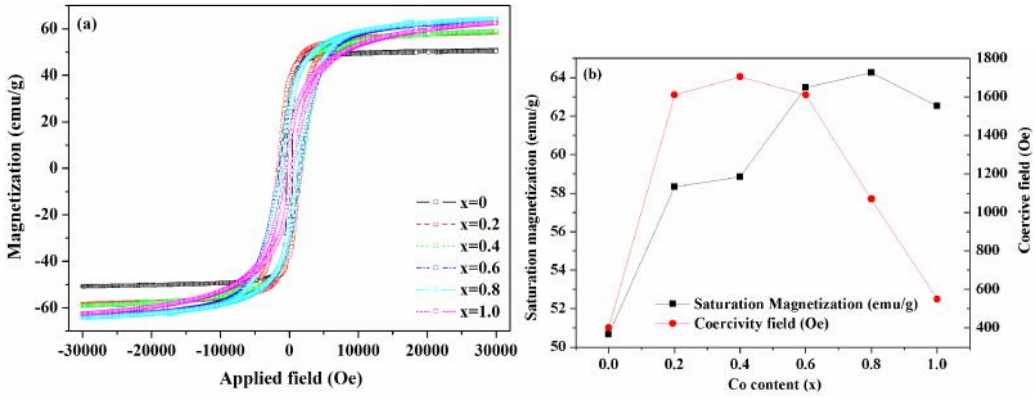

Figure 9. (a) Room temperature magnetic hysteresis loops of the $Ni_{1-x}Co_xFe_2O_4$ nanoparticles and (b) variations of saturation magnetization and coercivity with Co content.